

LETTER TO THE EDITOR

# The Milky Way Cepheid Leavitt law based on Gaia DR2 parallaxes of companion stars and host open clusters populations

Louise Breuval<sup>1</sup>, Pierre Kervella<sup>1</sup>, Richard I. Anderson<sup>2</sup>, Adam G. Riess<sup>3,4</sup>, Frédéric Arenou<sup>5</sup>, Boris Trahin<sup>1</sup>, Antoine Mérand<sup>2</sup>, Alexandre Gallenne<sup>6,7,8,9</sup>, Wolfgang Gieren<sup>7</sup>, Jesper Storm<sup>10</sup>, Giuseppe Bono<sup>11,12</sup>, Grzegorz Pietrzyński<sup>7,8</sup>, Nicolas Nardetto<sup>6</sup>, Behnam Javanmardi<sup>1</sup>, Vincent Hodge<sup>6</sup>

<sup>1</sup> LESIA, Observatoire de Paris, Université PSL, CNRS, Sorbonne Université, Univ. Paris Diderot, Sorbonne Paris Cité, 5 place Jules Janssen, 92195 Meudon, France. e-mail: louise.breuval@obspm.fr

<sup>2</sup> European Southern Observatory, Karl-Schwarzschild-Str. 2, 85748 Garching, Germany

<sup>3</sup> Space Telescope Science Institute, 3700 San Martin Drive, Baltimore, MD 21218, USA

<sup>4</sup> Department of Physics and Astronomy, Johns Hopkins University, Baltimore, MD 21218, USA

<sup>5</sup> GEPI, Observatoire de Paris, Université PSL, CNRS, 5 Place Jules Janssen, 92190 Meudon, France

<sup>6</sup> Université Côte d'Azur, Observatoire de la Côte d'Azur, CNRS, Laboratoire Lagrange, France

<sup>7</sup> Universidad de Concepción, Departamento de Astronomía, Casilla 160-C, Concepción, Chile

<sup>8</sup> Nicolaus Copernicus Astronomical Centre, Polish Academy of Sciences, Bartycka 18, 00-716 Warszawa, Poland

<sup>9</sup> Unidad Mixta Internacional Franco-Chilena de Astronomía (CNRS UMI 3386), Departamento de Astronomía, Universidad de Chile, Camino El Observatorio 1515, Las Condes, Santiago, Chile

<sup>10</sup> Leibniz-Institut für Astrophysik Potsdam (AIP), An der Sternwarte 16, 14482 Potsdam, Germany

<sup>11</sup> Department of Physics, Università di Roma Tor Vergata, via della Ricerca Scientifica 1, I-00133 Roma, Italy

<sup>12</sup> INAF-Osservatorio Astronomico di Roma, via Frascati 33, I-00040 Monte Porzio Catone, Italy

Received... ; accepted...

## ABSTRACT

**Aims.** Classical Cepheids provide the foundation for the empirical extragalactic distance ladder. Milky Way Cepheids are the only stars of this class accessible to trigonometric parallax measurements. However, the parallaxes of Cepheids from the second Gaia data release (GDR2) are affected by systematics due to the absence of chromaticity correction and occasionally by saturation.

**Methods.** As a proxy for the parallaxes of 36 Galactic Cepheids, we adopt either the GDR2 parallaxes of their spatially resolved companions or the GDR2 parallax of their host open cluster. This novel approach allows us to bypass the systematics on the GDR2 Cepheids parallaxes that is induced by saturation and variability. We adopt a GDR2 parallax offset of 0.046 mas with an uncertainty of 0.015 mas that covers most of the recent estimates.

**Results.** We present new Galactic calibrations of the Leavitt law in the  $V$ ,  $J$ ,  $H$ ,  $K_S$  and Wesenheit  $W_H$  bands. We compare our results with previous measurements from the Hubble Space Telescope (HST) and compute a revised value for the Hubble constant anchored to Milky Way Cepheids.

**Conclusions.** From an initial Hubble constant of  $76.18 \pm 2.37 \text{ km s}^{-1} \text{ Mpc}^{-1}$  based on parallax measurements without Gaia, we derive a revised value by adopting companion and average cluster parallaxes in place of direct Cepheid parallaxes and we find  $H_0 = 73.07 \pm 1.75 \text{ (stat. + syst.)} \pm 1.88 \text{ (ZP)} \text{ km s}^{-1} \text{ Mpc}^{-1}$  when all Cepheids are considered, and  $H_0 = 73.51 \pm 1.76 \text{ (stat. + syst.)} \pm 1.91 \text{ (ZP)} \text{ km s}^{-1} \text{ Mpc}^{-1}$  for fundamental mode pulsators only.

**Key words.** parallaxes – stars: distances – stars: variables: Cepheids – cosmology: distance scale

## 1. Introduction

Classical Cepheids (CCs) have historically a major importance among variable stars because of the simple correlation between their pulsation period and their intrinsic luminosity, also called the Leavitt law or the period-luminosity (hereafter PL) relation (Leavitt 1908; Leavitt & Pickering 1912). However, after more than a century of active research, the absolute calibration of the Leavitt law is still unsatisfactory due to the lack of precise and direct distance measurements for a sizeable sample these stars. A careful calibration of this relation and especially of its zero-point is fundamental, as it is used to anchor extragalactic distances and to derive the expansion rate of the Universe, i.e. the Hubble constant  $H_0$ . In fact, the determination of  $H_0$  from the Cosmic Microwave Background (CMB) based on the standard  $\Lambda$ -Cold-

Dark-Matter ( $\Lambda$ CMD) model (Planck Collaboration et al. 2018) is currently found to be in  $\sim 5\sigma$  tension with the empirical or direct distance ladder measurements (Riess 2019). This tension may have important implications in cosmology, and may even point towards new physics beyond  $\Lambda$ CMD (Verde et al. 2019).

The Leavitt law calibration requires the independent and accurate distance measurement for a sample of CCs. Unfortunately, Gaia's second data release (hereafter GDR2) contains a number of systematic effects that may reduce the precision of the parallaxes of CCs (Gaia Collaboration et al. 2018). First, CCs are bright stars, so a small number with  $G < 6 \text{ mag}$  are affected by saturation, making their parallaxes unreliable. In addition, CC colors cycle through many variations during the parallax cycle: the effective temperature of a Cepheid changes on average by 1000 K over a full pulsation cycle, which means  $\sim 0.5 \text{ mag}$  in op-

tical bands, so this may add additional noise to their astrometry due to the chromaticity of the PSF. Future Gaia data releases are expected to include chromaticity corrections for variable stars and incorporate a better model of the PSF to deal with saturation. While recent analyses of Gaia DR2 parallaxes for CCs with  $G > 6$  mag do not appear to suffer excess noise (Groenewegen 2018; Riess et al. 2018b; Gaia Collaboration et al. 2017; Clementini et al. 2019), it is important to pursue alternative approaches to extract parallaxes from Gaia DR2 for CCs that are insensitive to these systematics.

Even in the absence of systematic errors, the use of open cluster parallaxes for CCs they host can provide enhanced precision over the use of a single CC parallax. Because open cluster parallaxes are based on many stars, the increased precision from averaging as well as the ability to reject outliers for stars in astrometric binaries is extremely valuable.

In the present letter, we seek to calibrate the Milky Way (MW) Cepheid Leavitt law using stars that are not affected by these issues and to benefit from the gain in precision afforded by cluster average parallaxes. In Sect. 2, we introduce our sample of stars and their associated parallaxes. In Sect. 3.1, we derive calibrations of the Leavitt law in various bands. Then, in Sect. 3.2, we compare our GDR2 parallaxes with the corresponding expected parallaxes from Hubble Space Telescope (HST) measurements and in Sect. 3.3 we derive a value for the Hubble constant anchored to Milky Way Cepheids.

## 2. Sample of parallaxes

We consider two sets of parallaxes: one based on Cepheid companions and one based on average cluster parallaxes. The benefits of these samples are flux and color constancy (companions and clusters) and averaging over a large sample (clusters).

### 2.1. Parallaxes of Cepheids resolved companions

Recently, Kervella et al. (2019) presented a sample of 28 Galactic Cepheids that are members of gravitationally bound and spatially resolved stellar systems. In these systems, Cepheid companions are photometrically stable stars and their GDR2 parallaxes are therefore not affected by such a strong chromatic effect as Cepheids. As the CCs and their companions share the same parallax (their relative distance is negligible compared to the distance to Gaia), the GDR2 parallaxes of the companions provide a natural proxy for those of the CCs. The companions parallaxes are precise at 15% in average.

The angular separation between the CCs and their companions is in most cases larger than 10 arcsec, which is large enough to prevent flux contamination, given the brightness of the CCs. At 10" separation for stars hundreds to thousands of parsec distant, there is no expected effect of orbital motion on parallax or proper motion measurements: the parallaxes of the CCs and companions are not sensitive to the binarity of these wide systems.

The GDR2 astrometry is generally of poor quality for very bright stars ( $G < 6$  mag), due to calibration issues and saturation (Riess et al. 2018b; Drimmel et al. 2019; Lindegren 2019). This occurs independently of the chromaticity issue raised previously, whether the star is variable or not. While several Cepheids of our sample are close to this limit, with an average  $G$  magnitude of 8 mag, their companions are in average 7 mag fainter than their parent Cepheids. The companions are therefore not as affected as CCs by the saturation issue and they are far off from the sen-

sitivity limit. They consequently belong to the best dynamical range for *Gaia*.

We perform a selection based on GDR2 quality criteria and pulsation modes (see Appendix A.2 and C) that results in a sample of 22 GDR2 parallaxes of Cepheids resolved companions, listed in Table A.1.

### 2.2. Parallaxes of Cepheids in Open Clusters

Open clusters (OCs) contain a significant number of stars located at the same distance and are numerous in the Milky Way. Therefore, identifying Cepheids in OCs allows us to estimate their distances, with a gain in precision by taking the average over a population compared to individual parallax measurements. We performed a cross-match between the Ripepi et al. (2019) reclassification of GDR2 Cepheids and the Cantat-Gaudin et al. (2018) catalog of Milky Way Open Clusters. This catalog provides parallaxes for 1229 OCs that are precise at  $\sim 1\%$ , based on the GDR2 parallaxes of their member stars. Our comparison is based on 5 membership constraints: the separation  $\theta$ , parallax  $\varpi$ , proper motion  $\mu_\alpha^*$  and  $\mu_\delta$ , and age. More details on the data and the cross-match are given in Appendix A.2. This selection and a crossing with the literature resulted in a final sample of 14 cluster Cepheids, whose data are provided in Table A.2.

## 3. Results

### 3.1. Calibration of the Leavitt law

In this section, we combine the 22 Cepheids companions with the 14 open cluster Cepheids. Their parameters are listed in Table 1. The Leavitt law calibration is obtained by performing a fit of the Astrometry Based Luminosity function (ABL) on our sample, for which we applied a Monte Carlo simulation. More details on the method are provided in Appendix D.

We found 5 Cepheids to be present in both samples. For these 5 stars, the companion parallax and the cluster parallax agree within  $1\sigma$ , except for U Sgr that is at  $1.4\sigma$ . In order to avoid any correlation between our two sets of parallaxes, we recomputed for these 5 stars the Cantat-Gaudin et al. (2018) cluster parallaxes as the median of all stars parallaxes after excluding the companion. We found our new cluster parallaxes to differ by 0.5  $\mu\text{as}$  at most from the original values, so we adopted these new parallax values and considered the two sources of measurement to be independent and non-correlated. For these 5 Cepheids, both parallax measurements (cluster and companion) are considered independently in the linear fit.

GDR2 parallaxes are subject to a zero-point offset, whose value was studied extensively but is still debated. The different estimates are discussed in Appendix E. In the following, we adopt  $ZP_{\text{GDR2}} = -0.046$  mas (Riess et al. 2018b), which is close to the median of all values (see Table E.1).

In order to correct for the extinction, different formulations are available (Savage & Mathis 1979; Cardelli et al. 1989). We adopt the Fitzpatrick (1999) formulation with  $R_V = 3.3$ , that yields  $R_I = 0.86$ ,  $R_H = 0.55$ , and  $R_K = 0.37$ . This will allow a direct comparison of our calibration with that of Riess et al. (2016), based on HST Fine Guidance Sensor (FGS) and HST Wide Field Camera 3 (WFC3) measurements.

The PL coefficients obtained in different bands for  $ZP_{\text{GDR2}} = -0.046$  mas are listed in Table 2. For different  $ZP_{\text{GDR2}}$  values, the coefficients are provided in Table E.2 in the Appendix. The Leavitt law calibration in the  $K_S$  band is displayed in Fig. 1. The lower panel shows residuals in terms of parallax, computed as

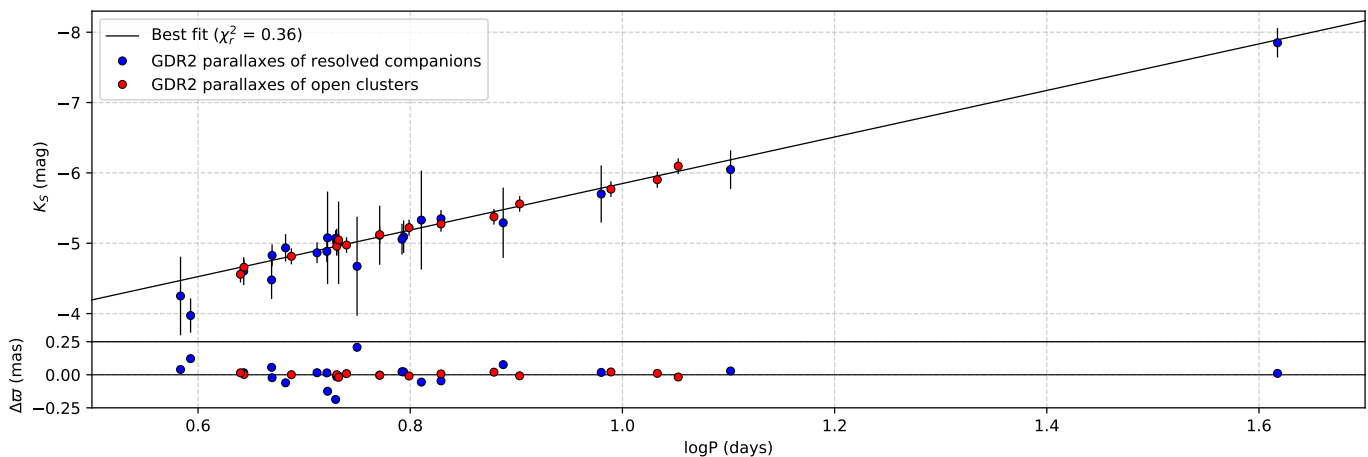


**Fig. 1.** Period-luminosity diagram in the  $K_s$  band calibrated with GDR2 parallaxes of Cepheids companions (blue) and open clusters (red).

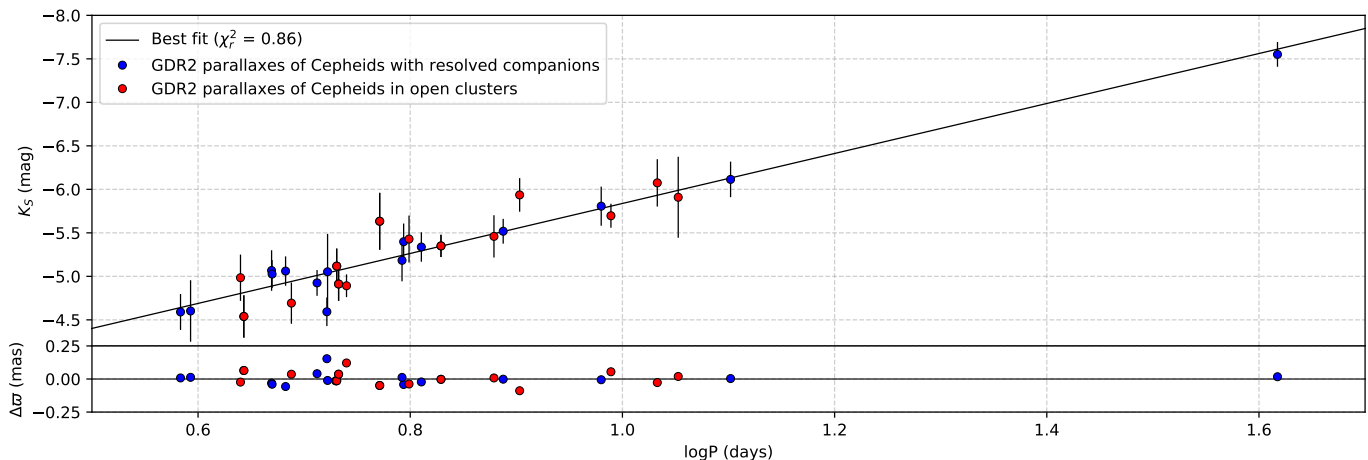


**Fig. 2.** Same as Fig. 1 but using directly GDR2 parallaxes of Cepheids.

the difference between the input parallax and the parallax given by the best fit. This calibration gives a reduced  $\chi^2$  of 0.36 and a dispersion of  $\sigma = 0.14$  mag.

An equivalent calibration, based this time on direct Cepheid parallaxes, is presented in Fig. 2. When the CC parallaxes are adopted, we obtain  $\chi_r^2 = 0.86$  and a dispersion of  $\sigma = 0.19$  mag. The dispersion of the PL relation based on Cepheid parallaxes (Fig. 2) does not appear to be systematic, but rather results in a larger spread not accounted in the uncertainties. The PL coefficients derived from GDR2 parallaxes of Cepheids are provided in Table F.1.

### 3.2. Comparison between GDR2 and HST parallaxes

In this section, we compare our sample of GDR2 parallaxes with a set of parallaxes available before the *Gaia* era. Riess et al. (2016), hereafter R16, combined 10 Cepheid parallaxes from HST/FGS (Benedict et al. 2007) with three *Hipparcos* measurements and 2 Cepheids with parallaxes measured by spatial scanning with the HST/WFC3 (Riess et al. 2014; Casertano et al. 2016), and obtain:

$$M_H^W = -5.85 - 3.26(\log P - 1) \quad (1)$$

Associated with this Galactic PL relation, R16 derive a Hubble constant of  $H_{0,R16} = 76.18 \pm 2.37 \text{ km s}^{-1} \text{ Mpc}^{-1}$  in the Milky

Way. They finally combine this result with other geometric distance calibrations of Cepheids and conclude with a final value of  $73.24 \pm 1.74 \text{ km s}^{-1} \text{ Mpc}^{-1}$ . We use the PL calibration from R16 based on the Milky Way anchor to compute the predicted parallaxes  $\varpi_{R16}$  for each star of our sample:

$$5 \log \varpi_{R16} = M_H^W - m_H^W + 10 \quad (2)$$

where  $m_H^W$  is the apparent magnitude in the Wesenheit system corrected for the Count-Rate Non-Linearity (CRNL) effect (see Appendix B) and  $M_H^W$  is derived from Eq. 1. The choice of a  $R$  value in agreement with Riess et al. (2016) (see Sect. 3) ensures the consistency of this comparison. To account for the width of the instability strip ( $\sigma = 0.07$  mag) and for the photometric transformations from ground to HST system ( $\sigma = 0.06$  mag), we set the apparent magnitudes uncertainties to 0.09 mag. Fig. 3 shows the comparison between the GDR2 parallaxes of our sample corrected by a 0.046 mas offset and the predicted parallaxes from R16. The GDR2 parallaxes appear to be slightly underestimated compared with the predicted values, especially for Cepheids with large parallax values.

The prototype  $\delta$  Cep is particularly interesting for this study: it hosts a resolved companion with a GDR2 parallax and it is also present in the sample of HST/FGS parallaxes by Benedict et al. (2007). The GDR2 parallax of its companion is  $3.393 \pm 0.049$  mas while its HST/FGS parallax is  $3.66 \pm 0.15$  mas. These two measurements differ by  $1.7\sigma$  (7% in relative terms), which

**Table 1.** Final sample adopted, combining Cepheids with resolved companions and open clusters Cepheids. Parallaxes in the first part of the table are from GDR2 for the companions, and parallaxes in the second part are from [Cantat-Gaudin et al. \(2018\)](#) based on GDR2. Reddenings  $E(B - V)$  are taken from the DDO database ([Fernie et al. 1995](#)), to which we applied a multiplicative factor of 0.94. Mean apparent magnitudes in  $V, J, H, K_S$  bands are from the catalog compiled by [Groenewegen \(2018\)](#):  $V$  band magnitudes are originally from [Mel'nik et al. \(2015\)](#) and NIR magnitudes are given in the 2MASS system with the original references provided in the last column. Apparent magnitudes in the  $W_H$  system are also provided, their uncertainties include the photometric transformation errors.

Cepheid	$P$ (days)	$\varpi^{(*)}$ (mas)	$E(B - V)$	$V$ (mag)	$J$ (mag)	$H$ (mag)	$K_S$ (mag)	$W_H^{(**)}$ (mag)	ref <sub>NIR</sub>
Sample of Cepheids with resolved companions									
DF Cas	3.832	0.367 $\pm$ 0.104	0.564 $\pm$ 0.049	10.880 $\pm$ 0.030	8.488 $\pm$ 0.025	8.036 $\pm$ 0.025	7.879 $\pm$ 0.025	7.533 $\pm$ 0.066	G14
CM Sct	3.917	0.518 $\pm$ 0.056	0.775 $\pm$ 0.045	11.100 $\pm$ 0.030	8.300 $\pm$ 0.025	7.818 $\pm$ 0.025	7.558 $\pm$ 0.025	7.240 $\pm$ 0.066	G14
EV Sct	4.396 $\star$	0.481 $\pm$ 0.040	0.623 $\pm$ 0.015	10.130 $\pm$ 0.030	7.608 $\pm$ 0.008	7.184 $\pm$ 0.008	7.018 $\pm$ 0.008	6.658 $\pm$ 0.061	L92
TV CMa	4.670	0.426 $\pm$ 0.054	0.574 $\pm$ 0.029	10.590 $\pm$ 0.030	8.022 $\pm$ 0.008	7.582 $\pm$ 0.008	7.364 $\pm$ 0.008	7.048 $\pm$ 0.061	M11
V532 Cyg	4.675 $\star$	0.619 $\pm$ 0.033	0.519 $\pm$ 0.007	9.090 $\pm$ 0.030	6.863 $\pm$ 0.025	6.393 $\pm$ 0.025	6.250 $\pm$ 0.025	5.919 $\pm$ 0.066	2MASS
V950 Sco	4.814 $\star$	0.893 $\pm$ 0.069	0.251 $\pm$ 0.019	7.310 $\pm$ 0.030	5.681 $\pm$ 0.008	5.439 $\pm$ 0.008	5.295 $\pm$ 0.008	5.083 $\pm$ 0.061	G18
V350 Sgr	5.154	1.015 $\pm$ 0.048	0.308 $\pm$ 0.008	7.470 $\pm$ 0.030	5.625 $\pm$ 0.010	5.245 $\pm$ 0.010	5.121 $\pm$ 0.010	4.844 $\pm$ 0.061	W84
VW Cru	5.265	0.679 $\pm$ 0.034	0.640 $\pm$ 0.046	9.600 $\pm$ 0.030	6.805 $\pm$ 0.025	6.261 $\pm$ 0.025	6.051 $\pm$ 0.025	5.681 $\pm$ 0.066	G14
AX Cir	5.273	1.725 $\pm$ 0.527	0.265 $\pm$ 0.121	5.880 $\pm$ 0.030	4.299 $\pm$ 0.025	3.879 $\pm$ 0.025	3.780 $\pm$ 0.025	3.524 $\pm$ 0.066	G14
$\delta$ Cep	5.366	3.364 $\pm$ 0.049	0.075 $\pm$ 0.018	3.950 $\pm$ 0.030	2.683 $\pm$ 0.010	2.396 $\pm$ 0.010	2.294 $\pm$ 0.010	2.104 $\pm$ 0.061	B97
CV Mon	5.379	0.508 $\pm$ 0.040	0.705 $\pm$ 0.018	10.310 $\pm$ 0.030	7.314 $\pm$ 0.008	6.781 $\pm$ 0.008	6.529 $\pm$ 0.008	6.165 $\pm$ 0.061	M11
QZ Nor	5.401 $\star$	0.452 $\pm$ 0.132	0.289 $\pm$ 0.020	8.870 $\pm$ 0.030	7.085 $\pm$ 0.008	6.748 $\pm$ 0.008	6.614 $\pm$ 0.008	6.360 $\pm$ 0.061	L92
V659 Cen	5.622	1.355 $\pm$ 0.448	0.151 $\pm$ 0.034	6.620 $\pm$ 0.030	5.177 $\pm$ 0.025	4.907 $\pm$ 0.025	4.651 $\pm$ 0.025	4.583 $\pm$ 0.066	G14
CS Vel	5.905	0.222 $\pm$ 0.050	0.716 $\pm$ 0.027	11.700 $\pm$ 0.030	8.771 $\pm$ 0.008	8.246 $\pm$ 0.008	8.011 $\pm$ 0.008	7.643 $\pm$ 0.061	L92
RS Nor	6.198	0.449 $\pm$ 0.043	0.577 $\pm$ 0.036	10.000 $\pm$ 0.030	7.412 $\pm$ 0.010	6.794 $\pm$ 0.010	6.683 $\pm$ 0.010	6.249 $\pm$ 0.061	SPIPS
X Cru	6.220	0.609 $\pm$ 0.061	0.294 $\pm$ 0.019	8.400 $\pm$ 0.030	6.521 $\pm$ 0.025	6.125 $\pm$ 0.025	5.935 $\pm$ 0.025	5.717 $\pm$ 0.066	G14
AW Per	6.464	1.046 $\pm$ 0.349	0.479 $\pm$ 0.016	7.480 $\pm$ 0.030	5.213 $\pm$ 0.008	4.832 $\pm$ 0.008	4.657 $\pm$ 0.008	4.354 $\pm$ 0.061	M11
U Sgr	6.745	1.461 $\pm$ 0.038	0.408 $\pm$ 0.007	6.690 $\pm$ 0.030	4.506 $\pm$ 0.008	4.100 $\pm$ 0.008	3.912 $\pm$ 0.008	3.637 $\pm$ 0.061	M11
ER Car	7.720	0.889 $\pm$ 0.210	0.111 $\pm$ 0.016	6.820 $\pm$ 0.030	5.310 $\pm$ 0.008	5.034 $\pm$ 0.008	4.896 $\pm$ 0.008	4.698 $\pm$ 0.061	G18
SX Vel	9.550	0.432 $\pm$ 0.086	0.237 $\pm$ 0.014	8.290 $\pm$ 0.030	6.500 $\pm$ 0.008	6.133 $\pm$ 0.008	5.991 $\pm$ 0.008	5.743 $\pm$ 0.061	L92
SY Nor	12.646	0.414 $\pm$ 0.053	0.611 $\pm$ 0.059	9.500 $\pm$ 0.030	6.574 $\pm$ 0.008	6.105 $\pm$ 0.008	5.865 $\pm$ 0.008	5.504 $\pm$ 0.061	G18
RS Pup	41.443	0.503 $\pm$ 0.045	0.451 $\pm$ 0.010	7.010 $\pm$ 0.030	4.365 $\pm$ 0.008	3.828 $\pm$ 0.008	3.619 $\pm$ 0.008	3.276 $\pm$ 0.061	L92
Sample of open cluster Cepheids									
CG Cas	4.365	0.282 $\pm$ 0.004	0.667 $\pm$ 0.009	11.380 $\pm$ 0.030	8.903 $\pm$ 0.025	8.299 $\pm$ 0.025	8.109 $\pm$ 0.025	7.775 $\pm$ 0.066	G14
EV Sct	4.398 $\star$	0.468 $\pm$ 0.004	0.623 $\pm$ 0.015	10.130 $\pm$ 0.030	7.608 $\pm$ 0.008	7.184 $\pm$ 0.008	7.018 $\pm$ 0.008	6.658 $\pm$ 0.061	L92
CF Cas	4.875	0.269 $\pm$ 0.004	0.556 $\pm$ 0.021	11.060 $\pm$ 0.030	8.590 $\pm$ 0.008	8.126 $\pm$ 0.008	7.900 $\pm$ 0.008	7.608 $\pm$ 0.061	M11
CV Mon	5.379	0.523 $\pm$ 0.010	0.705 $\pm$ 0.018	10.310 $\pm$ 0.030	7.314 $\pm$ 0.008	6.781 $\pm$ 0.008	6.529 $\pm$ 0.008	6.165 $\pm$ 0.061	M11
QZ Nor	5.401 $\star$	0.443 $\pm$ 0.002	0.289 $\pm$ 0.020	8.870 $\pm$ 0.030	7.085 $\pm$ 0.008	6.748 $\pm$ 0.008	6.614 $\pm$ 0.008	6.360 $\pm$ 0.061	L92
V Cen	5.495	1.288 $\pm$ 0.003	0.265 $\pm$ 0.016	6.820 $\pm$ 0.030	5.019 $\pm$ 0.008	4.642 $\pm$ 0.008	4.498 $\pm$ 0.008	4.249 $\pm$ 0.061	L92
CS Vel	5.905	0.221 $\pm$ 0.004	0.716 $\pm$ 0.027	11.700 $\pm$ 0.030	8.771 $\pm$ 0.008	8.246 $\pm$ 0.008	8.011 $\pm$ 0.008	7.643 $\pm$ 0.061	L92
V367 Sct	6.293	0.467 $\pm$ 0.004	1.145 $\pm$ 0.043	11.610 $\pm$ 0.030	7.605 $\pm$ 0.008	6.955 $\pm$ 0.008	6.651 $\pm$ 0.008	6.152 $\pm$ 0.061	L92
U Sgr	6.745	1.514 $\pm$ 0.003	0.408 $\pm$ 0.007	6.690 $\pm$ 0.030	4.506 $\pm$ 0.008	4.100 $\pm$ 0.008	3.912 $\pm$ 0.008	3.636 $\pm$ 0.061	M11
RS Ori	7.567	0.553 $\pm$ 0.004	0.332 $\pm$ 0.010	8.410 $\pm$ 0.030	6.398 $\pm$ 0.008	6.020 $\pm$ 0.008	5.860 $\pm$ 0.008	5.589 $\pm$ 0.061	M11
DL Cas	8.001	0.511 $\pm$ 0.002	0.487 $\pm$ 0.005	8.970 $\pm$ 0.030	6.550 $\pm$ 0.008	6.101 $\pm$ 0.008	5.892 $\pm$ 0.008	5.593 $\pm$ 0.061	M11
S Nor	9.754	1.025 $\pm$ 0.004	0.182 $\pm$ 0.008	6.420 $\pm$ 0.030	4.674 $\pm$ 0.008	4.288 $\pm$ 0.008	4.149 $\pm$ 0.008	3.905 $\pm$ 0.061	L92
TW Nor	10.786	0.383 $\pm$ 0.006	1.190 $\pm$ 0.023	11.670 $\pm$ 0.030	7.442 $\pm$ 0.008	6.712 $\pm$ 0.008	6.375 $\pm$ 0.008	5.865 $\pm$ 0.061	L92
V340 Nor	11.288	0.443 $\pm$ 0.002	0.312 $\pm$ 0.009	8.370 $\pm$ 0.030	6.211 $\pm$ 0.008	5.745 $\pm$ 0.008	5.573 $\pm$ 0.008	5.284 $\pm$ 0.061	L92

**References.** (G14) [Genovali et al. \(2014\)](#); [Genovali et al. \(2014\)](#); (L92) [Laney & Stobie \(1992\)](#); (M11) [Monson & Pierce \(2011\)](#); (2MASS) [Skrutskie et al. \(2006\)](#); (G18) [Groenewegen \(2018\)](#); (W84) [Welch et al. \(1984\)](#); (B97) [Barnes et al. \(1997\)](#); (SPIPS) Light curve fitting with the SPIPS algorithm ([Mérand et al. 2015](#)).

**Notes.** ( $\star$ ) Cepheid pulsating in the first-overtone mode. In that case, the period was converted following the approach described in Appendix C.

( $\ast$ ) The parallaxes presented in this Table do not include the parallax zero-point offset term.

( $\ast\ast$ )  $W_H$  apparent magnitudes presented in this Table do not include the addition of the CRNL term described in Appendix B.

agrees with the general trend observed in Fig. 3. We note that  $\delta$  Cep has no valid parallax in GDR2, so its companion parallax is the only possible alternative to HST/FGS measurements.

### 3.3. Implications on the distance scale

The determination of the Hubble constant by [Planck Collaboration et al. \(2018\)](#) exhibit a tension at the  $\sim 5\sigma$  level with the latest empirical estimate by [Riess et al. \(2019a\)](#) based on LMC Cepheids combined with masers in NGC 4258 and Milky Way parallaxes measured by the HST.

Following the method presented in Section 4 in [Riess et al. \(2018a\)](#), we translate our previous parallax comparison into a comparison in terms of the Hubble constant. We want to examine the impact of changing the MW anchor alone on the  $H_0$  measurement that depends on three anchors. Hence, we look at the  $H_0$  value from R16 that pertains only to the MW. We use the relation  $H_{0,GDR2} = \alpha H_{0,R16}$  where  $\alpha = \varpi_{GDR2}/\varpi_{R16}$  and  $H_{0,R16}$  is the value anchored to Milky Way Cepheids only and is equal to  $76.18 \pm 2.37 \text{ km s}^{-1} \text{ Mpc}^{-1}$ .

For each star of the sample, we derive the corresponding  $\alpha$  value and we adopt a Monte Carlo approach to estimate the final



**Table 2.** PL relations obtained with GDR2 parallaxes of Cepheid companions and open cluster Cepheids, for a parallax zero-point offset of  $-0.046$  mas. The equations are of the form  $M = a(\log P - 0.84) + b$  and  $\rho$  is the correlation between  $a$  and  $b$ .

Band	$a$	$b$	$\rho$	$\chi_r^2$	$\sigma$
$V$	$-2.459_{\pm 0.233}$	$-3.728_{\pm 0.046}$	0.16	0.30	0.18
$J$	$-3.087_{\pm 0.157}$	$-4.915_{\pm 0.026}$	0.20	0.54	0.16
$H$	$-3.232_{\pm 0.157}$	$-5.218_{\pm 0.025}$	0.20	0.39	0.16
$K_S$	$-3.310_{\pm 0.160}$	$-5.320_{\pm 0.025}$	0.20	0.36	0.14
$W_H$	$-3.367_{\pm 0.144}$	$-5.425_{\pm 0.022}$	0.20	0.57	0.16

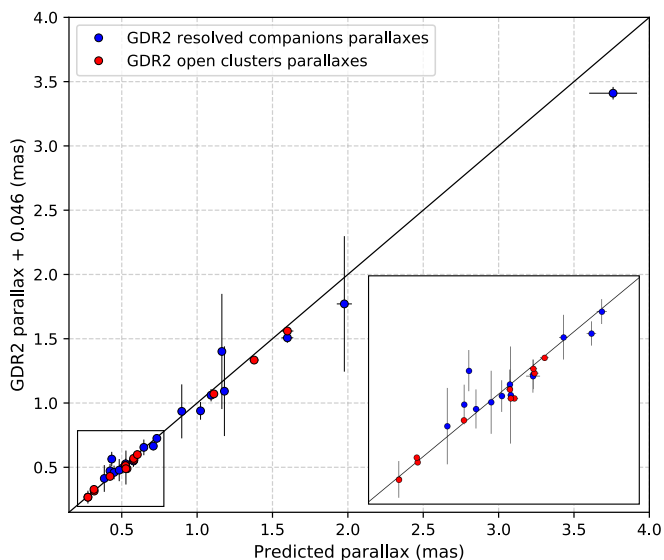


**Fig. 3.** Comparison of GDR2 parallaxes of resolved companions and open clusters hosting Cepheids with the predicted parallaxes using the MW PL calibration from R16, given in Eq. 1. The solid black line corresponds to the identity line.

average  $\alpha$  value of the sample. We performed this calculation on different samples and listed the resulting  $H_0$  values in Table 3. The uncertainties on  $H_0$  include the final error on the R16 estimate excluding the anchors (1.8%), the error on the estimation of  $\alpha$  and finally the uncertainties on the photometric relations to convert ground-based magnitudes into HST magnitudes (1.5%). Changing the GDR2 parallax offset by 0.015 mas results in a change of 2.6% in the Hubble constant, therefore, we adopted a confidence interval of 0.015 mas around the  $-0.046$  mas zero-point and added a 2.6% uncertainty to account for this effect.

**Table 3.** Hubble constant value derived from the comparison between our GDR2 parallax samples and the predicted parallaxes from R16. The first uncertainties are the statistics combined with the systematics, and the second ones account for the effect of the GDR2 parallax zero-point.

	$H_0$ ( $\text{km s}^{-1} \text{Mpc}^{-1}$ )	$H_0$ ( $\text{km s}^{-1} \text{Mpc}^{-1}$ )
	FU only	FU + FO
Companions	$72.65 \pm 2.15 \pm 1.89$	$72.36 \pm 2.07 \pm 1.88$
Clusters	$73.58 \pm 1.77 \pm 1.91$	$73.14 \pm 1.75 \pm 1.90$
<b>All Cepheids</b>	<b><math>73.51 \pm 1.76 \pm 1.91</math></b>	<b><math>73.07 \pm 1.75 \pm 1.90</math></b>

**Notes.** "FU" = Fundamental mode Cepheids;  
"FO" = First Overtone mode Cepheids with fundamentalized period.

We obtain a final value of  $73.51 \pm 2.60 \text{ km s}^{-1} \text{Mpc}^{-1}$  for fundamental modes only and of  $73.07 \pm 2.58 \text{ km s}^{-1} \text{Mpc}^{-1}$  for all stars included. Both values are very consistent with the LMC and NGC 4258 anchor results derived by Riess et al. (2019a), and also very close to the result by Reid et al. (2019). The last value agrees at the  $1.1 \sigma$  level with that of Freedman et al. (2020) and at the  $2.2$  level with the Planck Collaboration et al. (2018) measurement.

We note that the CCs used to calibrate the PL relation and  $H_0$  have lower mean periods than most extragalactic Cepheids found by HST. Though there is no evidence of a break in the PL relation at  $\log P = 1$  for the  $W_H$  magnitude system (Riess et al. 2016), it remains important to add longer period Cepheids to the parallax calibration to maintain low systematics.

## 4. Conclusions

We presented an original calibration of the Milky Way Leavitt law based on GDR2 parallaxes of resolved Cepheid companions and on GDR2 parallaxes of open clusters hosting Cepheids. Companion and cluster members are not subject to large amplitude photometric and color variability, which reduces the potential for systematic parallax uncertainties. Additionally, average cluster parallaxes established for solid cluster member stars allows to improve the precision by a factor  $\sqrt{N}$  where  $N$  is the number of member stars and is generally larger than 100. The comparison of our calibration with a previous work based on HST Cepheid parallaxes indicates a systematic offset between both measurements. By replacing the trigonometric parallaxes used in R16 by companion and cluster average parallaxes, we render the Milky Way, the LMC, and NGC4258 Leavitt Laws more consistent with one another: we find a MW estimate of  $73.51 \pm 2.60 \text{ km s}^{-1} \text{Mpc}^{-1}$  for fundamental modes only and of  $H_0 = 73.07 \pm 2.58 \text{ km s}^{-1} \text{Mpc}^{-1}$  for all stars included.

The inclusion of the variability of CCs is not expected in the astrometric processing of the third Gaia data release. However, the effects of the systematics due to the absence of chromaticity correction on Cepheids parallaxes should be reduced in the next releases thanks to the larger number of measurements. The future developments will help to pursue the community goal to measure  $H_0$  with utmost precision and accuracy.

*Acknowledgements.* We thank D. Graczyk, S. Borgniet and L. Inno for their comments that led to improvements of the present study. We are grateful to T. J. Calderwood from AAVSO for the photometry of Polaris. The research leading to these results has received funding from the European Research Council (ERC) under the European Union's Horizon 2020 research and innovation programme under grant agreement No 695099 (project CepBin). This work has made use of data from the European Space Agency (ESA) mission Gaia (<http://www.cosmos.esa.int/gaia>), processed by the Gaia Data Processing and Analysis Consortium (DPAC, <http://www.cosmos.esa.int/web/gaia/dpac/consortium>). Funding for the DPAC has been provided by national institutions, in particular the institutions participating in the Gaia Multilateral Agreement. The authors acknowledge the support of the French Agence Nationale de la Recherche (ANR), under grant ANR-15-CE31-0012-01 (project UnlockCepheids). W.G. and G.P. gratefully acknowledge financial support for this work from the BASAL Centro de Astrofísica y Tecnologías Afines (CATA) AFB-170002. W.G. acknowledges financial support from the Millennium Institute of Astrophysics (MAS) of the Iniciativa Científica Milenio del Ministerio de Economía, Fomento y Turismo de Chile, project IC120009. We acknowledge support from the IIdP II 2015 0002 64 and DIR/WK/2018/09 grants of the Polish Ministry of Science and Higher Education and Polish National Science Centre grants MAESTRO UMO-2017/26/A/ST9/00446. This research made use of Astropy7, a community-developed core Python package for Astronomy (Astropy Collaboration et al. 2018). We used the SIMBAD and VIZIER databases and catalogue access tool at the CDS, Strasbourg (France), and NASA's Astrophysics Data System Bibliographic Services.

## References

- Anderson, R. I. 2018, *A&A*, 611, L7
- Anderson, R. I., Eyer, L., & Mowlavi, N. 2013, *MNRAS*, 434, 2238
- Anderson, R. I., Saio, H., Ekström, S., Georgy, C., & Meynet, G. 2016, *A&A*, 591, A8
- Arenou, F. & Luri, X. 1999, in *Astronomical Society of the Pacific Conference Series*, Vol. 167, *Harmonizing Cosmic Distance Scales in a Post-HIPPARCOS Era*, ed. D. Egret & A. Heck, 13–32
- Arenou, F., Luri, X., Babusiaux, C., et al. 2018, *A&A*, 616, A17
- Astropy Collaboration, Price-Whelan, A. M., Sipőcz, B. M., et al. 2018, *AJ*, 156, 123
- Barnes, III, T. G., Fernley, J. A., Frueh, M. L., et al. 1997, *PASP*, 109, 645
- Benedict, G. F., McArthur, B. E., Feast, M. W., et al. 2007, *AJ*, 133, 1810
- Bond, H. E., Nelan, E. P., Remage Evans, N., Schaefer, G. H., & Harmer, D. 2018, *ApJ*, 853, 55
- Bono, G., Gieren, W. P., Marconi, M., & Fouqué, P. 2001, *ApJ*, 552, L141
- Cantat-Gaudin, T., Jordi, C., Vallenari, A., et al. 2018, *A&A*, 618, A93
- Cardelli, J. A., Clayton, G. C., & Mathis, J. S. 1989, *ApJ*, 345, 245
- Casertano, S., Riess, A. G., Anderson, J., et al. 2016, *ApJ*, 825, 11
- Clementini, G., Ripepi, V., Molinaro, R., et al. 2019, *A&A*, 622, A60
- Drimmel, R., Bucciarelli, B., & Inno, L. 2019, *Research Notes of the American Astronomical Society*, 3, 79
- Evans, N. R., Arellano Ferro, A., & Udalska, J. 1992, *AJ*, 103, 1638
- Feast, M. W. & Catchpole, R. M. 1997, *MNRAS*, 286, L1
- Fernie, J. D., Evans, N. R., Beattie, B., & Seager, S. 1995, *Information Bulletin on Variable Stars*, 4148
- Fitzpatrick, E. L. 1999, *PASP*, 111, 63
- Freedman, W. L., Madore, B. F., Hoyt, T., et al. 2020, *ApJ*, 891, 57
- Gaia Collaboration, Brown, A. G. A., Vallenari, A., et al. 2018, *A&A*, 616, A1
- Gaia Collaboration, Clementini, G., Eyer, L., et al. 2017, *A&A*, 605, A79
- Gallenne, A., Kervella, P., Evans, N. R., et al. 2018, *ApJ*, 867, 121
- Gallenne, A., Kervella, P., Mérand, A., et al. 2017, *A&A*, 608, A18
- Genovali, K., Lemasle, B., Bono, G., et al. 2014, *A&A*, 566, A37
- Graczyk, D., Pietrzyński, G., Gieren, W., et al. 2019, *ApJ*, 872, 85
- Groenewegen, M. A. T. 2018, *A&A*, 619, A8
- Hall, O. J., Davies, G. R., Elsworth, Y. P., et al. 2019, *MNRAS*, 1036
- Kervella, P., Bond, H. E., Cracraft, M., et al. 2014, *A&A*, 572, A7
- Kervella, P., Gallenne, A., Evans, N. R., et al. 2019, *A&A*, 623, A117
- Kervella, P., Trahin, B., Bond, H. E., et al. 2017, *A&A*, 600, A127
- Kharchenko, N. V., Piskunov, A. E., Roeser, S., Schilbach, E., & Scholz, R. D. 2013, *VizieR Online Data Catalog*, J/A+A/558/A53
- Koen, C., Marang, F., Kilkeny, D., & Jacobs, C. 2007, *MNRAS*, 380, 1433
- Kovtyukh, V., Lemasle, B., Chekhonadskikh, F., et al. 2016, *MNRAS*, 460, 2077
- Kovtyukh, V. V., Luck, R. E., Chekhonadskikh, F. A., & Belik, S. I. 2012, *MNRAS*, 426, 398
- Laney, C. D. & Stobie, R. S. 1992, *A&AS*, 93, 93
- Leavitt, H. S. 1908, *Annals of Harvard College Observatory*, 60, 87
- Leavitt, H. S. & Pickering, E. C. 1912, *Harvard College Observatory Circular*, 173, 1
- Lindgren, L. 2018, *Re-normalising the astrometric chi-square in Gaia DR2*, Tech. Rep. GAIA-C3-TN-LU-LL-124, Lund Observatory
- Lindgren, L. 2019, *arXiv e-prints*, arXiv:1906.09827
- Lindgren, L., Hernández, J., Bombrun, A., et al. 2018, *A&A*, 616, A2
- Luck, R. E. 2018, *AJ*, 156, 171
- Macri, L. M., Stanek, K. Z., Bersier, D., Greenhill, L. J., & Reid, M. J. 2006, *ApJ*, 652, 1133
- Madore, B. F. 1982, *ApJ*, 253, 575
- Madore, B. F., Freedman, W. L., & Moak, S. 2017, *ApJ*, 842, 42
- Mel'nik, A. M., Rautiainen, P., Berdnikov, L. N., Dambis, A. K., & Rastorguev, A. S. 2015, *Astronomische Nachrichten*, 336, 70
- Mérand, A., Kervella, P., Breitfelder, J., et al. 2015, *A&A*, 584, A80
- Monson, A. J. & Pierce, M. J. 2011, *ApJS*, 193, 12
- Muraveva, T., Delgado, H. E., Clementini, G., Sarro, L. M., & Garofalo, A. 2018, *MNRAS*, 481, 1195
- Planck Collaboration, Aghanim, N., Akrami, Y., et al. 2018, *arXiv e-prints* [arXiv:1807.06209]
- Reid, M. J., Pesce, D. W., & Riess, A. G. 2019, *ApJ*, 886, L27
- Riess, A. G. 2019, *Nature Reviews Physics*, 2, 10
- Riess, A. G., Casertano, S., Anderson, J., MacKenty, J., & Filippenko, A. V. 2014, *ApJ*, 785, 161
- Riess, A. G., Casertano, S., Yuan, W., et al. 2018a, *ApJ*, 855, 136
- Riess, A. G., Casertano, S., Yuan, W., et al. 2018b, *ApJ*, 861, 126
- Riess, A. G., Casertano, S., Yuan, W., Macri, L. M., & Scolnic, D. 2019a, *ApJ*, 876, 85
- Riess, A. G., Macri, L. M., Hoffmann, S. L., et al. 2016, *ApJ*, 826, 56
- Riess, A. G., Narayan, G., & Calamida, A. 2019b, *Calibration of the WFC3-IR Count-rate Nonlinearity, Sub-percent Accuracy for a Factor of a Million in Flux*, Tech. rep., Space Telescope Science Institute, 3700 San Martin Drive, Baltimore, MD 21218, USA
- Ripepi, V., Molinaro, R., Musella, I., et al. 2019, *A&A*, 625, A14
- Romaniello, M., Primas, F., Mottini, M., et al. 2008, *A&A*, 488, 731
- Sahlholdt, C. L. & Silva Aguirre, V. 2018, *MNRAS*, 481, L125
- Savage, B. D. & Mathis, J. S. 1979, *ARA&A*, 17, 73
- Schechter, P. L., Avruch, I. M., Caldwell, J. A. R., & Keane, M. J. 1992, *AJ*, 104, 1930
- Schönrich, R., McMillan, P., & Eyer, L. 2019, *MNRAS*, 487, 3568
- Skrutskie, M. F., Cutri, R. M., Stiening, R., et al. 2006, *AJ*, 131, 1163
- Stassun, K. G. & Torres, G. 2018, *ApJ*, 862, 61
- Turner, D. G. 2010, *Ap&SS*, 326, 219
- Turner, D. G. & Majaess, D. J. 2006, in *Canadian Astronomical Society Annual Meeting*, poster presentation
- Usenko, I. A., Kniazev, A. Y., Berdnikov, L. N., & Kravtsov, V. V. 2014, *Astronomy Letters*, 40, 800
- Verde, L., Treu, T., & Riess, A. G. 2019, *Nature Astronomy*, 3, 891
- Welch, D. L., Wieland, F., McAlary, C. W., et al. 1984, *ApJS*, 54, 547
- Zabolotskikh, M. V., Rastorguev, A. S., & Egorov, I. E. 2004, in *Astronomical Society of the Pacific Conference Series*, Vol. 316, *Order and Chaos in Stellar and Planetary Systems*, ed. G. G. Byrd, K. V. Kholshevnikov, A. A. Myllri, I. I. Nikiforov, & V. V. Orlov, 209
- Zinn, J. C., Pinsonneault, M. H., Huber, D., & Stello, D. 2019, *ApJ*, 878, 136

## Appendix A: Parallax samples

### Appendix A.1: Cepheids resolved companions sample

For a given Cepheid, when more than one companion was found by Kervella et al. (2019), we selected the companion with the smallest uncertainty on its parallax.

Various quality indicators are introduced in the second release of Gaia data, such as the re-normalised unit weight error (RUWE, noted  $\varrho$  in the following). It is particularly pertinent to use because it evaluates the quality of the parallax of a star compared to other stars of the same type. This parameter is defined by Lindegren (2018) as:

$$\varrho = \frac{\text{UWE}}{u_0(G, C)} \quad (\text{A.1})$$

where  $\text{UWE} = \sqrt{\chi^2/(N-5)}$  is the unit weight error and  $u_0$  is an empirical normalisation factor which is not directly available in the Gaia release but which can be computed from the lookup table on the ESA DR2 *Known issues* web page<sup>1</sup>. Following Lindegren (2018), we estimate that a parallax is reliable if  $\varrho < 1.4$ . The Table A.1 gives the RUWE for the Cepheids and the companions of our sample.

We note that some CCs from the Kervella et al. (2019) sample have no valid GDR2 parallax ( $\delta$  Cep, R Cru,  $\alpha$  UMi), while all companions have a valid parallax. In the initial Kervella et al. (2019) sample of 28 Cepheids, five of them have  $\varrho > 1.4$ , while only 2 companions are in this case, R Cru and V1046 Cyg, with  $\varrho = 2.80$  and 1.51 respectively. We exclude these 2 stars from the sample of companions in order to keep accurate parallaxes only.

The star CE Cas B is a particular case because its companion, CE Cas A, is also a Cepheid. The two components of CE Cas are present in the GDR2, but with statistically different parallaxes ( $\varpi_A = 0.317 \pm 0.031$  mas;  $\varpi_B = 0.262 \pm 0.030$  mas). We exclude both stars from our sample as a precaution.

The star  $\alpha$  UMi is extremely bright, with  $K \approx 0.5$  mag. Therefore, measuring accurate photometry for this star is particularly challenging. It has no valid parallax in GDR2 and appears saturated in most catalogs (Skrutskie et al. 2006). The only accurate average magnitudes based on several pulsation cycles were found in the AAVSO database that provides  $J = 0.93 \pm 0.01$  mag and  $H = 0.67 \pm 0.01$  mag in the UKIRT system. Additionally, the uncertain pulsation mode as well as the age difference between the Cepheid and its companion raise questions concerning the properties of  $\alpha$  UMi and whether it should be included in PL-relation fits (Anderson 2018; Bond et al. 2018; Groenewegen 2018). We decided to exclude this star from our sample.

The Cepheid RS Pup has been studied in details by Kervella et al. (2014) who estimated its parallax to  $0.524 \pm 0.022$  mas, using polarimetric HST images of the light echoes propagating in its circumstellar nebula (see also Kervella et al. (2017)). We note that this independent estimate is in very good agreement with the GDR2 parallax of RS Pup companion ( $0.503 \pm 0.045$  mas), but differs by 0.060 mas from the GDR2 parallax of the Cepheid itself ( $0.584 \pm 0.026$  mas).

A comparison between direct GDR2 Cepheid parallaxes and GDR2 companion parallaxes is displayed in Fig. A.1.

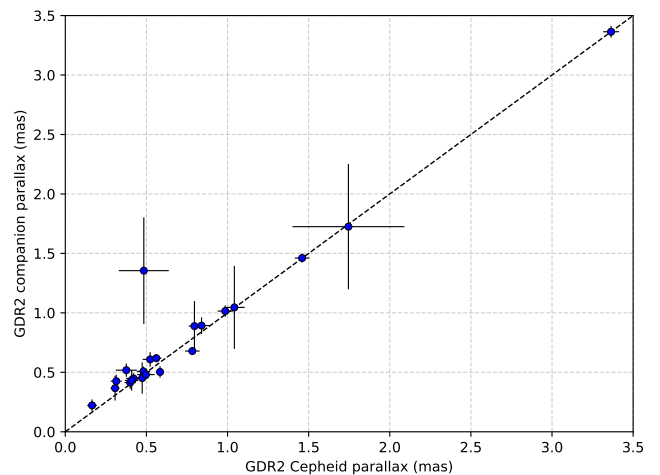


Fig. A.1. GDR2 parallaxes of our sample of companions as a function of the corresponding GDR2 Cepheid parallax.

### Appendix A.2: Cluster Cepheids sample

Following Anderson et al. (2013), we start the search for potential cluster members by looking at the proximity in the sky: we selected all Cepheids located in a region of  $10r_{50}$  around each cluster (where  $r_{50}$  is the radius containing half of the members) and we find a total of 2647 couples. For these couples, we compared the parallaxes, the proper motions and the age of both component. Since GDR2 parallaxes of Cepheids may be affected by systematics due to the absence of chromaticity correction, we account for this effect by including 20% error in quadrature. The proper motions for Cepheids and open clusters are taken from Ripepi et al. (2019) and Cantat-Gaudin et al. (2018) respectively. The age of open clusters is provided by Kharchenko et al. (2013), and the age of Cepheid is derived using period-age relations from Anderson et al. (2016).

We also searched in the literature for additional combinations and examined if they satisfy our membership constraints. Indeed, some Cepheids are not present in the Ripepi et al. (2019) reclassification, so they could not be found by means of our cross-match. Anderson et al. (2013) previously presented many of our couples, and provide 3 additional combinations that verify our membership criteria: TW Nor, CV Mon and V0367 Sct respectively in Lyngå 6, vdBergh 1 and NGC 6649.

We find a total of 14 Cepheids being candidate members of open clusters. They are listed in Table A.2, where filled circles stands for the agreement of a parameter at  $1\sigma$  or less. In this table is also provided the separation in arcmin between a Cepheid and the center of its host cluster. The field charts of each open cluster Cepheid is displayed in Fig. A.2, A.3 and A.4.

The Cepheid QZ Nor is a particular case: located at 18 arcmin of NGC 6067, it is a peripheral member of this cluster. The  $9\sigma$  difference in  $\mu_\delta$  could be explained by the fact that the Cepheid is leaving the cluster. This membership was identified by Anderson et al. (2013) as bona fide. Moreover, QZ Nor is also present in the sample of companions found by Kervella et al. (2019): the stable star Gaia DR2 5932565899990412672 is located at  $16''$  (30 kau) from the Cepheid. Its GDR2 parallax of  $0.452 \pm 0.132$  mas agrees particularly well with the  $0.443 \pm 0.002$  mas parallax of NGC 6067 from Cantat-Gaudin et al. (2018). Therefore, we decide not to exclude this couple.

The cross-match also resulted in potential members that only have 2MASS single epoch photometry available. Since average

<sup>1</sup> <https://www.cosmos.esa.int/web/gaia/dr2-known-issues>

**Table A.1.** Sample of Cepheids in resolved binary systems taken from [Kervella et al. \(2019\)](#): parameters of the Cepheids and of their stable companions. The symbol  $\varrho$  is the RUWE quality indicator from GDR2. (\*) indicates that  $\varrho > 1.4$ .

Cepheid	$\varpi_{\text{GDR2}}$ (mas)	$\varrho$	$G$ (mag)	Companion (GDR2)	$\varpi_{\text{GDR2}}$ (mas)	$\varrho$	$G$ (mag)
DF Cas	0.307 $\pm$ 0.028	0.98	10.434 $\pm$ 0.0001	465719182408531072	0.367 $\pm$ 0.104	1.12	17.259 $\pm$ 0.0009
CM Sct	0.376 $\pm$ 0.065	1.02	10.510 $\pm$ 0.0005	4253603428053877504	0.518 $\pm$ 0.056	0.95	14.728 $\pm$ 0.0005
EV Sct	0.497 $\pm$ 0.054	1.05	9.622 $\pm$ 0.0002	4156513016572003840	0.481 $\pm$ 0.040	1.03	13.615 $\pm$ 0.0015
TV CMa	0.314 $\pm$ 0.034	0.94	10.085 $\pm$ 0.0002	3044483895574944512	0.426 $\pm$ 0.054	1.12	15.771 $\pm$ 0.0029
V532 Cyg	0.561 $\pm$ 0.032	0.86	8.673 $\pm$ 0.0003	1971721839529622272	0.619 $\pm$ 0.033	0.93	14.674 $\pm$ 0.0004
V950 Sco	0.840 $\pm$ 0.052	1.09	7.052 $\pm$ 0.0007	5960623340819000192	0.893 $\pm$ 0.069	1.00	15.279 $\pm$ 0.0024
V350 Sgr	0.986 $\pm$ 0.047	0.92	7.251 $\pm$ 0.0002	4080121319521641344	1.015 $\pm$ 0.048	0.96	12.268 $\pm$ 0.0002
VW Cru	0.783 $\pm$ 0.045	0.98	9.014 $\pm$ 0.0003	6053622508133367680	0.679 $\pm$ 0.034	0.96	14.074 $\pm$ 0.0002
AX Cir	1.745 $\pm$ 0.345	10.3 *	5.626 $\pm$ 0.0006	5874031027625742848	1.725 $\pm$ 0.527	1.13	19.824 $\pm$ 0.0037
$\delta$ Cep	-	20.9 *	-	2200153214212849024	3.364 $\pm$ 0.049	0.85	6.282 $\pm$ 0.0005
CV Mon	0.482 $\pm$ 0.041	1.16	9.605 $\pm$ 0.0113	3127142327895572352	0.508 $\pm$ 0.040	1.03	13.489 $\pm$ 0.0003
QZ Nor	0.474 $\pm$ 0.038	1.01	8.577 $\pm$ 0.0001	593256589990412672	0.452 $\pm$ 0.132	1.02	17.935 $\pm$ 0.0013
V659 Cen	0.484 $\pm$ 0.154	4.52 *	6.391 $\pm$ 0.0003	5868451109212716928	1.355 $\pm$ 0.448	1.00	19.695 $\pm$ 0.0036
CS Vel	0.165 $\pm$ 0.030	1.01	11.103 $\pm$ 0.0002	5308893046071732096	0.222 $\pm$ 0.050	0.95	16.203 $\pm$ 0.0007
RS Nor	0.421 $\pm$ 0.046	0.99	9.485 $\pm$ 0.0005	5932812740361508736	0.449 $\pm$ 0.043	1.06	14.547 $\pm$ 0.0003
X Cru	0.523 $\pm$ 0.046	0.97	8.068 $\pm$ 0.0001	6059762524642419968	0.609 $\pm$ 0.061	1.16	16.045 $\pm$ 0.0006
AW Per	1.042 $\pm$ 0.064	1.06	7.048 $\pm$ 0.0011	174489098011144960	1.046 $\pm$ 0.349	1.07	17.417 $\pm$ 0.0030
U Sgr	1.460 $\pm$ 0.045	1.06	6.354 $\pm$ 0.0005	4092905203841177856	1.461 $\pm$ 0.038	0.90	11.141 $\pm$ 0.0006
ER Car	0.796 $\pm$ 0.035	0.95	6.606 $\pm$ 0.0002	5339394048386734336	0.889 $\pm$ 0.210	1.09	18.444 $\pm$ 0.0023
SX Vel	0.409 $\pm$ 0.041	1.00	7.973 $\pm$ 0.0003	5329838158460399488	0.432 $\pm$ 0.086	0.95	17.019 $\pm$ 0.0014
SY Nor	0.400 $\pm$ 0.035	1.10	8.965 $\pm$ 0.0006	5884729035245399424	0.414 $\pm$ 0.053	1.28	12.105 $\pm$ 0.0019
RS Pup	0.584 $\pm$ 0.026	0.97	6.459 $\pm$ 0.0003	5546476755539995008	0.503 $\pm$ 0.045	1.00	16.248 $\pm$ 0.0006

magnitudes are preferred for the Leavitt law calibration, we discarded these couples. In that case, we found V379 Cas, GU Nor and XZ Car to be members of NGC 129, NGC 6067 and NGC 3496 respectively.

A comparison between direct GDR2 Cepheid parallaxes and the corresponding open cluster parallaxes from [Cantat-Gaudin et al. \(2018\)](#) is displayed in Fig. A.5.

## Appendix B: Photometry

In order to determine the phase-averaged magnitudes of the CCs of our sample, we first searched them in the catalogue assembled by [Groenewegen \(2018\)](#). It is a compilation of mean apparent magnitudes in  $J$ ,  $H$ ,  $K$  and  $V$  bands in different photometric systems, taken from different sources (see Table 1). [Laney & Stobie \(1992\)](#) provides NIR magnitudes in the SAAO system, with uncertainties of 0.008 mag. For homogeneity, we converted them into the 2MASS system using the equations from [Koen et al. \(2007\)](#):

$$\begin{aligned} J_{2\text{MASS}} &= -0.028 + J_{\text{SAAO}} - 0.047(J_{\text{SAAO}} - K_{\text{SAAO}}) \\ H_{2\text{MASS}} &= +0.014 + H_{\text{SAAO}} \\ K_{2\text{MASS}} &= -0.015 + K_{\text{SAAO}} + 0.177(H_{\text{SAAO}} - K_{\text{SAAO}}) \\ &\quad - 0.082(J_{\text{SAAO}} - H_{\text{SAAO}})^2 \end{aligned}$$

The magnitudes given by [Monson & Pierce \(2011\)](#) are in the BIRCAM photometric system with uncertainties of 0.008 mag, and the magnitudes taken from [Welch et al. \(1984\)](#) and [Barnes et al. \(1997\)](#) are in the CIT photometric system. They were all converted into the 2MASS system using the equations from [Monson & Pierce \(2011\)](#):

$$\begin{aligned} K_{2\text{MASS}} &= K_{\text{BIRCAM}} + 0.008 (J_{\text{BIRCAM}} - K_{\text{BIRCAM}}) - 0.042 \\ J_{2\text{MASS}} &= K_{2\text{MASS}} + 1.052 (J_{\text{BIRCAM}} - K_{\text{BIRCAM}}) - 0.002 \\ H_{2\text{MASS}} &= K_{2\text{MASS}} + 0.993 (H_{\text{BIRCAM}} - K_{\text{BIRCAM}}) + 0.050 \end{aligned}$$

$$\begin{aligned} K_{2\text{MASS}} &= K_{\text{CIT}} + 0.001 (J_{\text{CIT}} - K_{\text{CIT}}) - 0.019 \\ J_{2\text{MASS}} &= K_{2\text{MASS}} + 1.068 (J_{\text{CIT}} - K_{\text{CIT}}) - 0.020 \\ H_{2\text{MASS}} &= K_{2\text{MASS}} + 1.000 (H_{\text{CIT}} - K_{\text{CIT}}) + 0.034 \end{aligned}$$

The NIR magnitudes from [Genovali et al. \(2014\)](#) are derived by template fitting and provided in the 2MASS system. For the remaining stars, the mean magnitude is computed as the median of the available data in [Welch et al. \(1984\)](#), [Schechter et al. \(1992\)](#) and 2MASS ([Skrutskie et al. 2006](#)). For RS Nor, the averaged NIR magnitudes were derived by fitting the photometric light curves using the SPIPS algorithm ([Mérand et al. 2015](#)). In the  $V$  band, all mean magnitudes are provided in the standard Johnson system and taken from [Mel'nik et al. \(2015\)](#). An uncertainty of 0.03 mag on those magnitudes is adopted.

From apparent magnitudes, we build the reddening-free Wesenheit magnitudes  $m_H^W$  ([Madore 1982](#)) which are a combination of HST bands defined by [Riess et al. \(2018a\)](#) as:

$$m_H^W = F160W - R(F555W - F814W) \quad (\text{B.1})$$

where  $R = 0.386$  is derived from the [Fitzpatrick \(1999\)](#) formulation with  $R_V = 3.3$ . The correspondance between HST filters  $F160W$ ,  $F555W$  and  $F814W$  and ground based magnitudes in  $J$ ,  $H$  and  $V$  is given by:

$$\begin{aligned} F160W &= H + 0.25 (J - H) - 0.030 \\ F555W &= V + 0.28 (J - H) + 0.020 \\ F814W &= V - 0.47 (V - H) - 0.035 \end{aligned}$$

These HST relations have a scatter of 0.06 mag and are computed with the average apparent  $J$ ,  $H$  and  $V$  magnitudes from Table 1.

We note that the transformation from ground-based magnitudes into the HST system requires to account for the Count-Rate Non-Linearity (CRNL) effect ([Riess et al. 2018b](#)). This bias affects the infrared detectors on WFC3 and has the consequence



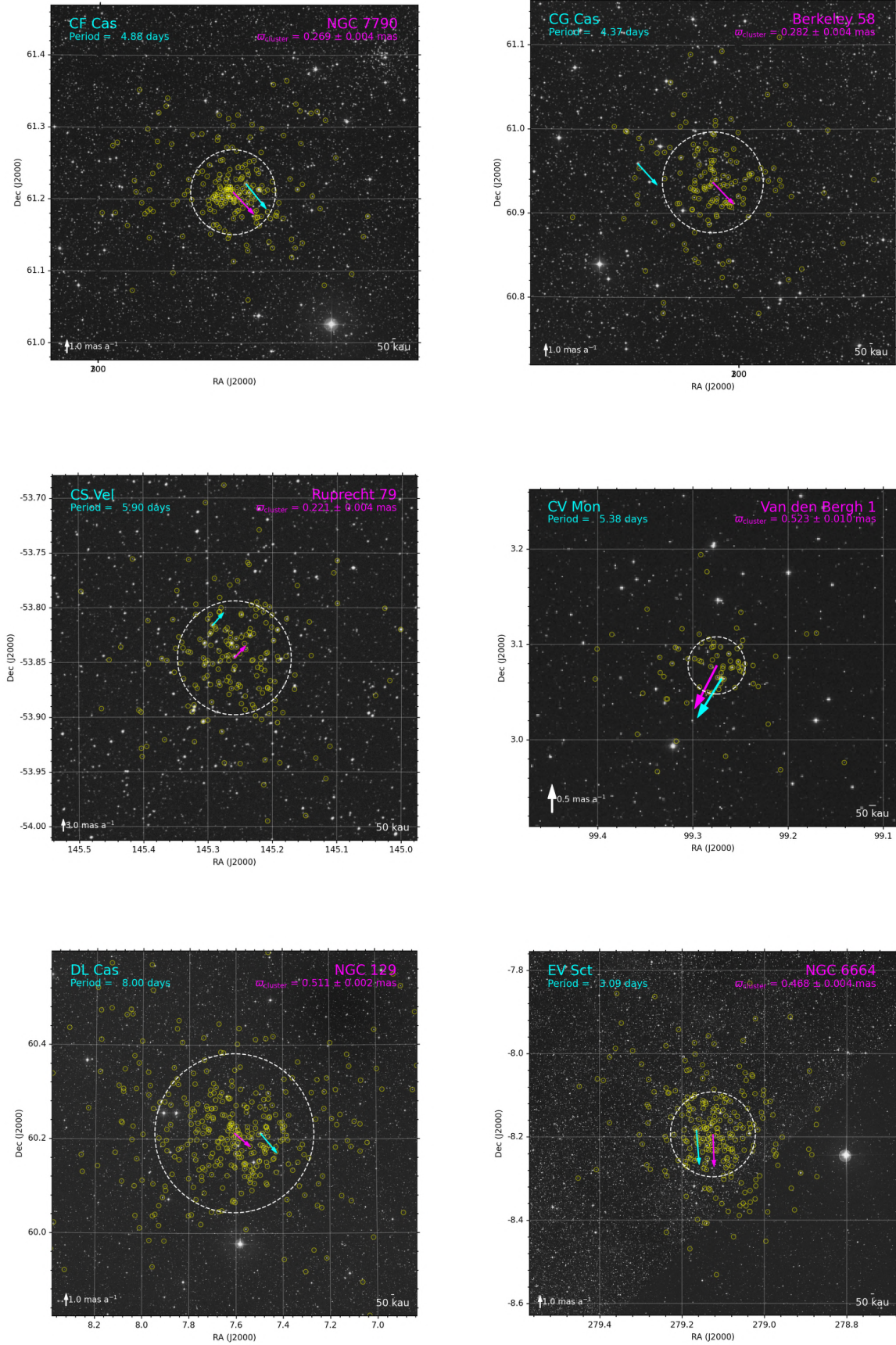


**Fig. A.2.** Field charts of our candidate Cepheids in their host clusters. The white dashed circles shows the radius  $r_{50}$  containing half of the cluster stars, and each yellow circle shows a cluster member. The blue and pink arrows shows the Cepheid and cluster proper motion, respectively.



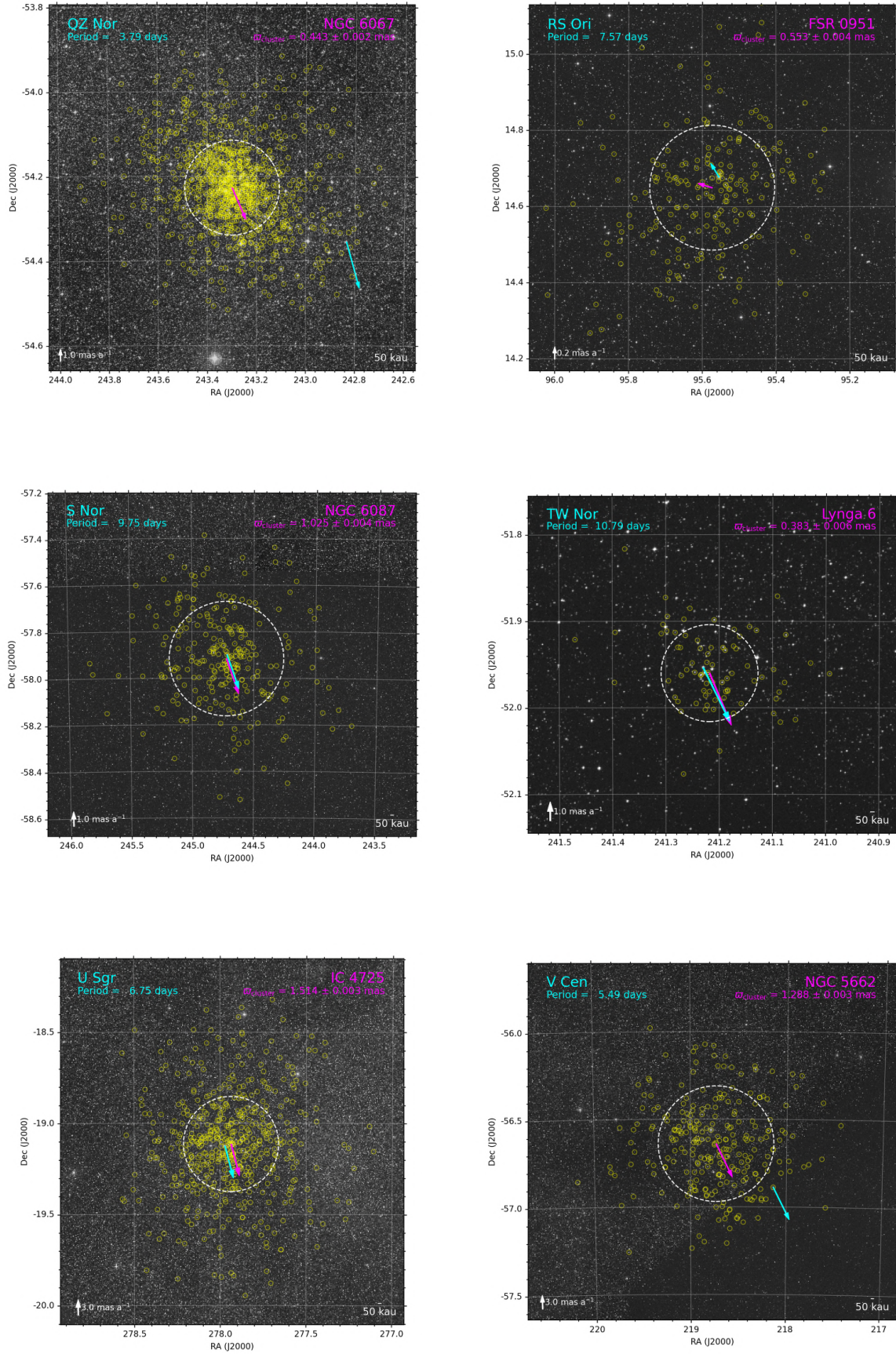
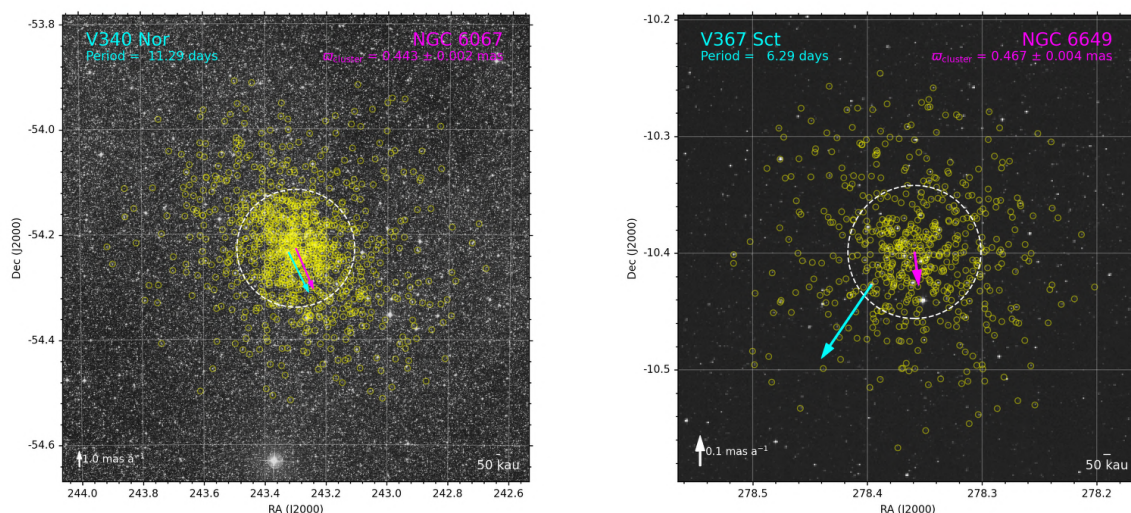


Fig. A.3. Continuation of Fig. A.2

**Table A.2.** Sample of cluster Cepheids found by our cross-match selection and in the literature. Full circles stand for an agreement smaller than  $1\sigma$  between the Cepheid and the cluster parameters.

Cepheid	Cluster	$\varpi$	$\mu_\alpha^*$	$\mu_\delta$	Age	Sep (')	Ref
CV Mon	vdBergh 1	●	●	●	●	0.9	A13
S Nor	NGC 6087	●	●	●	●	1.0	A13
U Sgr	IC 4725	●	●	●	●	2.1	A13
V367 Sct	NGC 6649	●	●	●	●	2.8	A13
V Cen	NGC 5662	●	●	●	●	25	A13
RS Ori	FSR 0951	●	●	●	$2.4 \sigma$	2.0	-
CS Vel	Ruprecht 79	●	●	●	$2.5 \sigma$	2.2	T10
DL Cas	NGC 129	●	●	$3.4 \sigma$	●	3.4	A13
EV Sct	NGC 6664	●	$1.1 \sigma$	●	●	2.4	A13
V340 Nor	NGC 6067	●	$1.3 \sigma$	●	●	0.9	A13
CF Cas	NGC 7790	●	$1.9 \sigma$	●	●	1.3	A13
TW Nor	Lyngå 6	●	$2.0 \sigma$	●	$1.4 \sigma$	0.6	A13
QZ Nor	NGC 6067	●	$1.2 \sigma$	$9 \sigma$	●	18	A13
CG Cas	Berkeley 58	●	$4.1 \sigma$	$2.0 \sigma$	$1.2 \sigma$	5.5	A13

**References.** (A13): [Anderson et al. \(2013\)](#); (T10): [Turner \(2010\)](#)



**Fig. A.4.** Continuation of Fig. A.3

of decreasing the magnitude of faint stars as extragalactic CCs, compared to bright stars as Milky Way CCs. This correction is performed by adding 0.026 mag to HST  $F160W$  apparent magnitudes ([Riess et al. 2019b](#)).

We also account for the width of the instability strip in the photometry errors. In the  $V$  band, [Macri et al. \(2006\)](#) find a dispersion of 0.23 mag: an intrinsic width is 0.22 mag and is obtained after subtracting the estimated measurement errors. For  $J$ ,  $H$  and  $K$  bands, [Madore et al. \(2017\)](#) finds a scatter of 0.12 mag, which leaves an intrinsic width of 0.11 mag in NIR bands. Finally, [Riess et al. \(2019a\)](#) find a dispersion of 0.075 mag in the  $W_H$  band, yielding an intrinsic width of 0.07 mag for the instability strip.

In order to compute absolute magnitudes, we need to correct the apparent magnitudes from the interstellar absorption. We take the  $E(B - V)$  values from the DDO database ([Fernie et al. 1995](#)), which is a compilation of various  $E(B - V)$  from the literature determined in the same system. Following [Groenewegen](#)

(2018), we apply a multiplicative factor of 0.94 to these reddening values.

## Appendix C: Pulsation modes

The identification of first overtone (FO) Cepheids is essential for the Leavitt law calibration. These stars belong to a parallel sequence on the PL plane and their pulsation period can be converted into a fundamentalized period ([Feast & Catchpole 1997](#); [Kovtuykh et al. 2016](#)). We review the different pulsation modes found in the literature for the stars of our sample. We followed the pulsation modes provided by different sources in literature, and in particular the reclassification from [Ripepi et al. \(2019\)](#).

The pulsation modes for the Cepheids of our sample are presented in Table C.1. The second and third column of this table give the pulsation mode provided by the GRD2 catalogue and the literature, respectively. The last column gives the adopted pulsation mode.



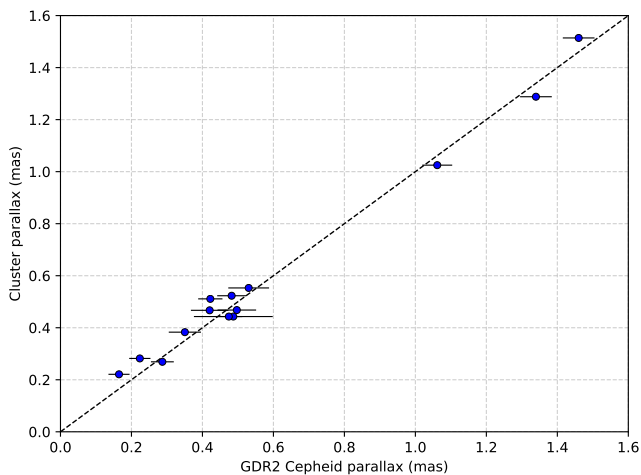


**Fig. A.5.** Parallaxes of our sample of cluster Cepheids from [Cantat-Gaudin et al. \(2018\)](#) as a function of the corresponding GDR2 Cepheid parallax.

For BP Cir and DK Vel, different pulsation modes were found: they are both classified as FO Cepheids by GDR2 and other studies ([Zabolotskikh et al. 2004](#); [Ripepi et al. 2019](#)), while they are listed as fundamentals by [Luck \(2018\)](#). The two stars are also consistent with fundamental pulsators in the PL plane. Given the disagreement between the different references about the pulsation mode of BP Cir and DK Vel, we decide to exclude them from the sample.

In order to establish accurate PL and PW relations without excluding the first overtones, we converted their observed periods  $P_{FO}$  into the fundamental mode equivalent period  $P_F$  using the equation by [Kovtyukh et al. \(2016\)](#):

$$P_{FO}/P_F = -0.0239_{\pm 0.0031} \log P_F - 0.0404_{\pm 0.0035} [\text{Fe}/\text{H}] + 0.7187_{\pm 0.0017}$$

Field and cluster Cepheids have a similar distribution in the Galactic plane, so they have similar metallicity distributions and both of them can be assumed close to solar ([Romaniello et al. 2008](#)). The first overtones of the sample have periods  $P_{FO}$  comprised between 3 and 4 days. In this range of periods, we can approximate the previous equation by the linear relation:

$$P_F = 1.4459 P_{FO} - 0.0736 \quad (\text{C.1})$$

The conversion of first overtones into fundamentals is listed in Table C.2. The positions of these Cepheids in the PL plane after the transformation are consistent with the distribution of fundamental pulsators.

Even though converting first overtones into fundamentals may introduce a small uncertainty on periods, we decide to include them in the sample for the calibration of the Leavitt law. Indeed, the periods obtained after conversion with the relations from [Feast & Catchpole \(1997\)](#) and [Kovtyukh et al. \(2016\)](#) only differ by 0.006 days. [Gallenne et al. \(2018\)](#) find a difference of less than 1% between an empirical conversion law and a theoretical one. Including the five first overtones of the sample with their modified periods instead of rejecting them induces only a very small change on the intercept of the PL relation and allows to improve the precision of the fit.

## Appendix D: Methods

In order to calibrate the PL relations as well as Period-Wesenheit (PW) relations, we used the approach introduced by [Feast &](#)

**Table C.1.** Pulsation mode of the Cepheids of our sample.

Cepheid	GDR2	Literature	Adopted
AW Per	FU	FU <sup>d,e</sup>	FU
AX Cir	FU	FU <sup>d,e</sup>	FU
BP Cir	FO	FU <sup>e</sup> , FO <sup>a,b,c,d</sup>	★
CF Cas	FU	FU <sup>d,e</sup>	FU
CG Cas	FU	FU <sup>d,e</sup>	FU
CM Sct	FU	FU <sup>d,e</sup>	FU
CS Vel	FU	FU <sup>d,e</sup>	FU
CV Mon	-	FU <sup>e</sup>	FU
δ Cep	-	FU <sup>e</sup>	FU
DF Cas	FU	FU <sup>d</sup>	FU
DL Cas	FU	FU <sup>d,e</sup>	FU
DK Vel	FO	FU <sup>e</sup> , FO <sup>a,d</sup>	★
ER Car	FU	FU <sup>d,e</sup>	FU
EV Sct	FO	FO <sup>d,e,i</sup>	FO
QZ Nor	FO	FU <sup>e</sup> , FO <sup>d</sup>	FO
RS Nor	FU	FU <sup>d,e</sup>	FU
RS Ori	FO	FU <sup>d,e</sup>	FU
RS Pup	FU	FU <sup>d,e</sup>	FU
S Nor	FU	FU <sup>d,e</sup>	FU
SX Vel	FU	FU <sup>d,e</sup>	FU
SY Nor	FU	FU <sup>d,e</sup>	FU
TV CMa	FU	FU <sup>d,e</sup>	FU
TW Nor	-	FU <sup>e</sup>	FU
U Sgr	FU	FU <sup>d,e</sup>	FU
V340 Nor	-	FU <sup>d,e</sup>	FU
V350 Sgr	FO	FU <sup>d,e</sup>	FU
V367 Sct	-	FU <sup>j</sup> , FO <sup>e</sup>	FU
V532 Cyg	FO	FU <sup>e</sup> , FO <sup>d</sup>	FO
V659 Cen	FU	FU <sup>e</sup> , FO <sup>a,d</sup>	FU
V950 Sco	FO	FU <sup>e</sup> , FO <sup>d</sup>	FO
V Cen	FU	FU <sup>d,e</sup>	FU
VW Cru	FU	FU <sup>d,e</sup>	FU
X Cru	FU	FU <sup>d,e</sup>	FU

**References.** (a) [Zabolotskikh et al. \(2004\)](#); (b) [Evans et al. \(1992\)](#); (c) [Usenko et al. \(2014\)](#); (d) [Ripepi et al. \(2019\)](#); (e) [Luck \(2018\)](#); (f) [Gallenne et al. \(2018\)](#); (g) [Kovtyukh et al. \(2012\)](#); (h) [Bono et al. \(2001\)](#); (i) [Turner & Majaess \(2006\)](#); (j) [Anderson et al. \(2013\)](#).

**Notes.** 'FU' = Fundamental; 'FO' = First Overtone; ★ = excluded because of uncertain pulsation mode.

**Table C.2.** Period conversion of first overtones into fundamental pulsators.

Cepheid	$P_{FO}$	$P_F$
EV Sct	3.091	4.396
V532 Cyg	3.284	4.675
V950 Sco	3.380	4.814
QZ Nor	3.786	5.401

[Catchpole \(1997\)](#) and [Arenou & Luri \(1999\)](#) and we computed the Astrometric Based Luminosity (ABL), defined as:

$$ABL = 10^{0.2M_\lambda} = \varpi 10^{0.2m_\lambda - 2} \quad (\text{D.1})$$

where  $M_\lambda$  is the absolute magnitude,  $m_\lambda$  is the dereddened apparent magnitude and  $\varpi$  is the parallax in milliarcseconds. Calibrating the Leavitt Law following this approach is equivalent to determine the coefficients  $a$  and  $b$  in the equation:

$$ABL = 10^{0.2[a(\log P - \log P_0) + b]} \quad (\text{D.2})$$



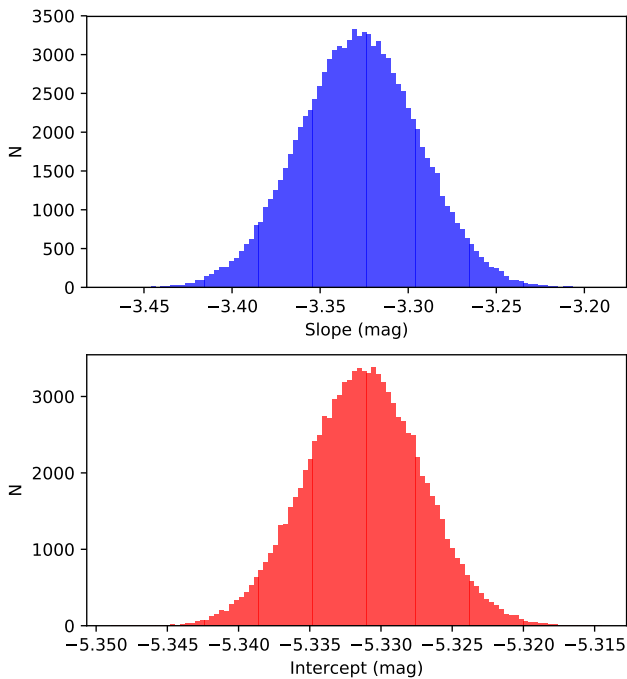


**Fig. D.1.** Distribution of slopes and zero-points obtained for the PL relation with the Monte Carlo approach in the  $K_S$  band.

We performed a weighted fit of the ABL function by using the `curve_fit` function from the python Scipy library. The robustness of the fit and of the uncertainties is ensured by a Monte Carlo approach, applied with 10 000 iterations. The distributions of the slope and zero-point of our  $K_S$  Leavitt law obtained by this technique are displayed on the histograms in Fig. D.1.

We used the formalism detailed in Gallenne et al. (2017), i.e. we adopted the following linear parametrization:

$$M_\lambda = b_\lambda + a_\lambda (\log P - \log P_0) \quad (\text{D.3})$$

where  $a_\lambda$  and  $b_\lambda$  are respectively the slope and the zero-point of the PL relation. Such a parametrization removes the correlation between  $a_\lambda$  and  $b_\lambda$  and minimizes their respective uncertainties. The optimum value of  $\log P_0$  depends on the dataset (see Gallenne et al. (2017) for further details):

$$\log P_0 = \frac{\langle \log P_i / e_i^2 \rangle}{\langle 1/e_i^2 \rangle} \quad (\text{D.4})$$

where  $\log P_i$  are the periods of the stars, and  $e_i$  are the uncertainties on their parallax;  $\langle \rangle$  denotes the averaging operator. We find our sample centered around  $\log P_0 = 0.84$ .

## Appendix E: Influence of GDR2 parallax zero-point

Together with the second Gaia data release, many authors found different parallax zero-point values. Lindegren et al. (2018) used quasars to derive that Gaia parallaxes are underestimated by 0.029 mas. This finding agrees with the value of -0.0319 mas found by Arenou et al. (2018) based on Milky Way Cepheids. From detached eclipsing binaries and surface brightness-color relations, Graczyk et al. (2019) derived a zero-point of -0.031 mas. Larger values were also found by Ripepi et al. (2019) and Stassun & Torres (2018), who find zero-point offsets of -0.070 mas and -0.082 mas respectively. Intermediary

**Table E.1.** Zero-point offset for GDR2 parallaxes found in the literature.

ZP <sub>GDR2</sub> (mas)	Reference	Type of sources
-0.029	L18	Quasars
-0.031 ± 0.011	G19	Eclipsing binaries
-0.0319 ± 0.0008	A18	MW Cepheids
-0.035 ± 0.016	SSA18	Dwarf stars
-0.041 ± 0.010	H19	Red giants
-0.046 ± 0.013	R18	MW Cepheids
-0.049 ± 0.018	G18	MW Cepheids
-0.053 ± 0.003	Z19	Red giants
-0.054 ± 0.006	S19	GDR2 RV
-0.057 ± 0.003	M18	RR Lyrae
-0.070 ± 0.010	R19	LMC Cepheids
-0.082 ± 0.033	ST18	Eclipsing binaries

**References.** (L18) Lindegren et al. (2018); (G19) Graczyk et al. (2019); (A18) Arenou et al. (2018); (SSA) Sahlholdt & Silva Aguirre (2018); (H19) Hall et al. (2019); (R18) Riess et al. (2018b); (G18) Groenewegen (2018); (Z19) Zinn et al. (2019); (S19) Schönrich et al. (2019); (M18) Muraveva et al. (2018); (R19) Ripepi et al. (2019); (ST18) Stassun & Torres (2018).

values were derived by Riess et al. (2018b) and Groenewegen (2018), who estimate -0.046 mas and -0.049 mas respectively. The recent determinations of ZP<sub>GDR2</sub> are listed in Table E.1.

Table E.2 gives the PL coefficients obtained with different parallax offsets. Changing the zero-point from -0.029 mas to -0.070 mas results in a change of 0.7% in slope and 2.8% (or 0.153 mag) in intercept for the  $K_S$  band PL relation. Both slope and intercept increase with this offset variation.

**Table E.2.** PL relations obtained with GDR2 parallaxes of resolved companions and open clusters, for different zero-point offsets. The equations are of the form  $M = a (\log P - 0.84) + b$ .

Band	$a$	$b$	$\rho$	$\chi_r^2$	$\sigma$
ZP <sub>GDR2</sub> = -0.029 mas					
$V$	-2.451 ± 0.235	-3.793 ± 0.047	0.16	0.28	0.18
$J$	-3.074 ± 0.158	-4.980 ± 0.026	0.20	0.48	0.16
$H$	-3.218 ± 0.158	-5.283 ± 0.025	0.20	0.38	0.16
$K_S$	-3.296 ± 0.158	-5.385 ± 0.025	0.20	0.36	0.14
$W_H$	-3.353 ± 0.144	-5.491 ± 0.022	0.21	0.51	0.16
ZP <sub>GDR2</sub> = -0.046 mas					
$V$	-2.459 ± 0.233	-3.728 ± 0.046	0.16	0.30	0.18
$J$	-3.087 ± 0.157	-4.915 ± 0.026	0.20	0.54	0.16
$H$	-3.232 ± 0.157	-5.218 ± 0.025	0.20	0.39	0.16
$K_S$	-3.310 ± 0.160	-5.320 ± 0.025	0.20	0.36	0.14
$W_H$	-3.367 ± 0.144	-5.425 ± 0.022	0.20	0.57	0.16
ZP <sub>GDR2</sub> = -0.070 mas					
$V$	-2.466 ± 0.237	-3.643 ± 0.046	0.16	0.36	0.19
$J$	-3.096 ± 0.157	-4.829 ± 0.025	0.20	0.77	0.17
$H$	-3.244 ± 0.157	-5.131 ± 0.025	0.20	0.56	0.17
$K_S$	-3.321 ± 0.159	-5.232 ± 0.025	0.21	0.52	0.15
$W_H$	-3.381 ± 0.143	-5.339 ± 0.022	0.21	0.88	0.17

## Appendix F: Period-Luminosity calibration from direct CC parallaxes

**Table F.1.** PL calibrations obtained with GDR2 parallaxes of Cepheid companions and open clusters hosting Cepheids, compared with the same calibration based on direct CC parallaxes. The equations are of the form  $M = a(\log P - 0.84) + b$ , with  $ZP_{\text{GDR2}} = -0.046$  mas.

Band	$a$	$b$	$\rho$	$\chi_r^2$	$\sigma$
Parallaxes of resolved companions and open clusters					
$V$	$-2.459_{\pm 0.233}$	$-3.728_{\pm 0.046}$	0.16	0.30	0.18
$J$	$-3.087_{\pm 0.157}$	$-4.915_{\pm 0.026}$	0.20	0.54	0.16
$H$	$-3.232_{\pm 0.157}$	$-5.218_{\pm 0.025}$	0.20	0.39	0.16
$K_S$	$-3.310_{\pm 0.160}$	$-5.320_{\pm 0.025}$	0.20	0.36	0.14
$W_H$	$-3.367_{\pm 0.144}$	$-5.425_{\pm 0.022}$	0.20	0.57	0.16
Cepheid parallaxes					
$V$	$-2.112_{\pm 0.235}$	$-3.829_{\pm 0.050}$	0.09	0.53	0.21
$J$	$-2.691_{\pm 0.153}$	$-4.987_{\pm 0.033}$	0.03	0.90	0.19
$H$	$-2.814_{\pm 0.152}$	$-5.278_{\pm 0.032}$	0.03	0.82	0.19
$K_S$	$-2.870_{\pm 0.153}$	$-5.378_{\pm 0.033}$	0.03	0.86	0.19
$W_H$	$-2.924_{\pm 0.142}$	$-5.483_{\pm 0.030}$	0.01	0.85	0.18